Keck Observations of Near-Earth Asteroids in the Thermal Infrared

Marco Delbó[1] **and Alan W. Harris**

DLR Institute of Planetary Research, Rutherfordstrasse 2, 12489 Berlin, Germany

E-mail: delbo@to.astro.it and alan.harris@dlr.de

Richard P. Binzel

Department of Earth, Atmospheric, and Planetary Sciences, MIT, Cambridge, Massachusetts 02139

Petr Pravec

Astronomical Institute, Academy of Sciences of the Czech Republic, CZ-25165 Ondřejov, Czech Republic

and

John K. Davies

Astronomy Technology Centre, Royal Observatory Edinburgh, Blackford Hill, Edinburgh EH9 3HJ, UK

Submitted to *Icarus*

REVISED VERSION

9 July 2003

[1] Present address: Osservatorio Astronomico di Torino, Strada Osservatorio 20, 10025 Pino Torinese (TO), Italy

No. of manuscript pages: 36

No. of figures: 3

No. of tables: 4

Running head: **Thermal-IR Observations of Near-Earth Asteroids**

Editorial correspondence to:

Alan W. Harris

DLR Dept. of Planetary Exploration

Rutherfordstrasse 2

12489 Berlin

Germany

Tel: +49 30 67055 324

Fax: +49 30 67055 340

E-mail: alan.harris@dlr.de

ABSTRACT

We present the results of thermal-infrared observations of 20 near-Earth asteroids (NEAs) obtained in the period March 2000 – February 2002 with the 10-m Keck-1 telescope on Mauna Kea, Hawaii. The measured fluxes have been fitted with thermal-model emission continua to determine sizes and albedos. This work increases the number of NEAs having measured albedos by 35%. The spread of albedos derived is very large (p_v = 0.02 – 0.55); the mean value is 0.25, which is much higher than that of observed main-belt asteroids. In most cases the albedos are in the ranges expected for the spectral types, although some exceptions are evident. Our results are consistent with a trend of increasing albedo with decreasing size for S-type asteroids with diameters below 20 km. A number of objects are found to have unexpectedly low apparent color temperatures, which may reflect unusual thermal properties. However, the results from our limited sample suggest that high thermal-inertia, regolith-free objects may be uncommon, even amongst NEAs with diameters of less than 1 km. We discuss the significance of our results in the light of information on these NEAs taken from the literature and the uncertainties inherent in applying thermal models to near-Earth asteroids.

Keywords: Asteroids, Infrared Observations, Photometry, Spectrophotometry

1. INTRODUCTION

More than 2200 near-Earth asteroids (NEAs) have been discovered to date. However, efforts to physically characterize NEAs are being outstripped by the discovery rate. Our understanding of the nature, origin and size distribution of the NEA population remains severely limited.

One of the most crucial physical parameters of an asteroid is its albedo, which allows the size to be determined given the visible absolute magnitude, *H*. Reliable albedo measurements are the key to understanding the mineralogy of NEAs and to establishing their size distribution, factors that are of vital importance in determining the origin of the NEA population and the magnitude of the terrestrial impact hazard. However, reliable albedos have been determined for relatively few NEAs so far. Excluding results derived from this work, Binzel *et al*. (2002) in their review of the physical properties of NEAs were able to assign a "measured" albedo to only 45 near-Earth asteroids. Estimates of the size distribution of the NEA population therefore still rely on assumed average values of albedo taken from studies of the main-belt population. Werner *et al*. (2002) considered size-dependent values of the visual geometric albedo, namely $p_v = 0.11$ and $p_v = 0.25$, for objects with diameters above and below about 1 km, respectively, in order to relate a number / size distribution to a number / absolute magnitude (*H*) distribution. Stuart (2001) used $p_v = 0.11$, while Bottke *et al*. (2000) assumed $p_v \approx 0.15$, to convert the observed *H*-frequency distribution to the size-frequency distribution of the NEA population.

Measurements of the thermal emission of an atmosphere-less object obtained at mid-IR wavelengths (5 -20 μm) and of its visible reflected light, combined with a suitable model of the surface thermal emission, allow the size and albedo of the object to be determined.

The Standard Thermal Model (STM, see Lebofsky *et al*. 1986, and references therein) is the basic and most widely used asteroid thermal model. It was designed for use with main-belt asteroids and is applicable to objects with low thermal inertia and/or rotating slowly, so that each surface element can be considered to be in instantaneous thermal equilibrium with solar insolation. For example, an asteroid covered in a dusty regolith would be expected to have low thermal inertia. A corresponding simple

model for the extreme case of high thermal inertia and/or fast rotation is the so-called fast rotating or isothermal latitude model (Lebofsky and Spencer 1989), hereafter FRM, in which the surface temperature distribution is a function of latitude only. An asteroid with a surface of bare rock would be expected to have a large thermal inertia. Using the STM or FRM the diameter and albedo can be calculated simultaneously on the basis of the different expressions relating these parameters to the observed thermal emission at a single wavelength, e.g. 10 μm, and reflected light. Veeder *et al*. (1989) reported diameters and albedos for 22 NEAs based on flux measurements at 10 μm interpreted in terms of the STM and FRM. However, Harris (1998) showed that neither the STM nor the FRM produce good fits in general to thermal-infrared continua of NEAs, which may be due to their having different surface properties than observed main-belt asteroids, perhaps because of their relatively small sizes and consequent lack of retention of collisional debris, and/or the fact that they are often observed at large solar phase angles for which these simple models were not designed. Harris (1998) proposed a solution in the form of a modified STM (the near-Earth asteroid thermal model, NEATM), which uses the information in the observed thermal continuum flux distribution to force the model temperature distribution to be consistent with the apparent color temperature of the asteroid. Unlike the STM and FRM, the NEATM requires measurements of the thermal flux at more than one wavelength. Of the three thermal models, the NEATM generally provides the most reliable results, judging from the comparison of resulting diameters and albedos with values derived by other means (see Harris and Lagerros 2002).

It is very instructive to test thermal models on NEAs because this population of asteroids has very broad ranges of size, shape, albedo, and other physical parameters, and observations can be made over a wide range of phase angle. Observations such as those discussed here enable the limitations of existing asteroid thermal models to be probed and lead to a greater understanding of how to interpret observed thermal emission in terms of the physical properties of asteroids.

Here we present the results of a campaign of thermal-infrared observations of NEAs with the Keck-I telescope. The unrivalled performance of the Keck I/Long Wave Spectrometer (LWS) combination in the thermal infrared provides access to a large number of NEAs and enables albedos and sizes of a significant number of sub-kilometer sized objects to be determined. The results obtained with the three

thermal models outlined above are presented for comparison and their implications for the physical properties of the observed asteroids are discussed.

2. OBSERVATIONS AND DATA REDUCTION

The observations were carried out at the Keck-1 telescope (R. P. Binzel, P. I.) on 7 nights between March 2000 and February 2002. Relevant parameters of the target asteroids are given in Table I. The Long Wavelength Spectrograph (LWS), a liquid-helium cooled instrument for imaging and spectroscopy in the range 5 – 20 μm installed at the forward Cassegrain focus, was used in imaging mode. Details of the instrument are given by Jones and Puetter (1993) and can be found on the Keck Observatory web site (www2.keck.hawaii.edu/inst/lws/lws.html). The 10.24" field was chopped and nodded with an amplitude of 10". Narrow-band filters centered on 4.8, 8.0, 8.9, 10.7, 11.7, 12.5, 17.6, 17.9 and 20.0 μm were used. The telescope was tracked at the rates predicted from the ephemerides of each target. Nevertheless, in a few cases resulting co-added images suffered a smearing effect due to small tracking errors, therefore nod sets were shifted and registered before co-adding where necessary to avoid compromising photometric accuracy.

An aperture photometry procedure based on the ATV package written in IDL by Aaron Barth (www.astro.caltech.edu/~barth/atv/) was used to derive raw flux data from the LWS images of the target asteroids and calibration stars. IDL was developed by Research Systems Inc. (www.rsinc.com/).

In each case calibration stars were chosen to be close on the sky to the target asteroid and the asteroid and the calibration stars were observed at similar airmasses as far as possible. Absolutely calibrated infrared spectra for the calibration stars were taken from the database of Cohen *et al*. (1999) and convolved with the filter-instrument profiles to give integrated absolute fluxes. Absolutely calibrated fluxes for the target asteroids were obtained by multiplying the integrated absolute fluxes of the calibration stars by the ratios of the target/calibration star raw counts in each filter. For those asteroids for which the observed flux distribution was well sampled, color corrections for the different flux

distributions of the calibration stars and asteroids in the filter passbands were performed but were found to be no more than a few percent.

Table I lists relevant observational circumstances and physical data for the target asteroids. The resulting fluxes are listed in Table II. The quoted uncertainties in the flux measurements refer to the statistical uncertainties in the synthetic aperture procedure only. Errors in the absolute calibration and fluctuations in atmospheric conditions during the observations increase the scatter in the flux data.

[TABLE I, TABLE II]

3. THERMAL-MODEL FITTING

In order to calculate diameters and geometric albedos, p_v, three different asteroid thermal models were fitted to the measured infrared fluxes: the standard thermal model (STM, Lebofsky *et al*. 1986), the fast rotating model (FRM, Lebofsky and Spencer 1989), and the near-Earth asteroid thermal model (NEATM, Harris 1998).

The STM assumes the asteroid is rotating slowly and has a low thermal inertia (or the Sun lies on its rotation axis) so that the temperature distribution is a simple function of the angular distance, φ, from the sub-solar point, at which the temperature distribution has its maximum, i. e.

$$T(\varphi) = T_0 \cos^{1/4}(\varphi). \quad (1)$$

The sub-solar temperature is given by

$$T_0 = [(1-A)\, S /(\eta\, \varepsilon\, \sigma)]^{1/4}, \quad (2)$$

where A is the bolometric Bond albedo, S the solar flux at the asteroid, η the beaming parameter, ε the emissivity, and σ the Stefan-Boltzmann constant. The temperature is assumed to fall to zero at the terminator and there is no thermal emission from the night side. The beaming parameter was originally introduced to allow the model temperature distribution to be modified to take account of the observed

enhancement of thermal emission at small solar phase angles due to surface roughness. In practice, η can be thought of as a modeling parameter that allows a first-order correction for any effect such as beaming, thermal inertia and rotation that influences the surface temperature distribution presented to the observer. An empirical coefficient of 0.01 mag deg^{-1} is used to correct fluxes for the phase effect (which leads to a decrease in observed flux with increasing phase angle) for phase angles up to about 30°; it is considered unreliable beyond 30°. The STM has been calibrated at 10 μm against the occultation diameters of the large main-belt asteroids Ceres and Pallas, leading to the adoption of 0.756 for the value of η (Lebofsky *et al*. 1986). The STM should therefore give accurate results for an asteroid that has thermal properties similar to those of large main-belt asteroids and is observed at a small phase angle. In any case, the STM results should normally provide a lower limit on the size and an upper limit on the albedo.

The FRM applies to the opposite extreme case of a fast rotating object and/or one with a high thermal inertia. The spin axis is assumed to be perpendicular to the plane containing the Sun, the asteroid and the observer. The temperature distribution of the FRM depends only on latitude and no phase correction is required. There is equal thermal emission from the day and night sides.

The NEATM, which is an adaptation of the STM, differs from the older model in making use of *multi-wavelength* thermal-infrared data to solve simultaneously for the beaming parameter, size, and albedo. This is important in the case of near-Earth asteroids, which may have surface properties differing considerably from those of large main-belt asteroids and are often observed at large phase angles. At small phase angles the effect of surface roughness is to increase the thermal flux observed (the so-called “beaming effect”) and decrease the value of η to less than unity, the value applicable in the case of a perfectly smooth sphere. At large phase angles observers see less thermal emission and a lower color temperature as a result of the beaming effect (note that in contrast to the NEATM, the STM takes no account of the reduction in color temperature with increasing phase angle). On the other hand, significant thermal inertia has the opposite effect: the temperature contrast around the body is reduced, leading to lower flux values and a lower color temperature (higher η) being observed at low phase angles. The model is used to calculate numerically the thermal flux an observer would detect from the illuminated portion of a sphere visible at a given solar phase angle and value of η. The NEATM, like the

STM, assumes that no emission originates on the night side of the object, an assumption that would be expected to lead to overestimation of diameters and underestimation of albedos at very high solar phase angles for objects with high thermal inertia. In such cases the FRM may be the more appropriate model to use. In principle the NEATM can be applied to any object for which adequate thermal-infrared data are available for model fitting to the thermal continuum, and in most cases it should be more accurate than the STM or FRM. For more detailed discussions of the thermal models outlined here see Harris (1998), Harris and Lagerros (2002), and Delbó and Harris (2002), and references therein. The latter work gives the mathematical expressions for calculating the wavelength-dependent observable thermal-infrared fluxes for all three models.

Application of all three thermal models gives some idea of the modeling uncertainties involved. Flux data and thermal model fits for 12 of the asteroids observed are plotted in Fig. 1.

In a number of cases in which the data are of poor quality, or observations were made over a small wavelength range, the NEATM fits and the resulting η-values are not well constrained. In these cases default values of η were used, based on the distribution of the points in Fig. 2 (see Section 6). The default values used are $\eta = 1.0$ for $\alpha < 45°$ and $\eta = 1.5$ for $\alpha > 45°$.

The resulting diameters, albedos and η-values are given in Table III. Previously published results for NEAs based on good quality data and NEATM fits are listed in Table IV.

[FIGURE 1]

[TABLE III, TABLE IV]

4. UNCERTAINTIES

Due to its rotation the observed thermal flux of an asteroid changes continuously as a function of time. Measurements carried out at different times refer in general to different rotational phases. A correction can be performed if visible lightcurve data are available for the time of the thermal observations. We have lightcurve-corrected the measured flux values to the mean lightcurve magnitude in those cases in which adequate optical data are available, on the assumption that the optical and thermal-infrared lightcurves are identical. However, differences between the two lightcurves, in phase, amplitude and

structure, cannot be ruled out and may contribute significantly to the scatter of the flux data plotted in Fig. 1. In some cases no lightcurve data covering the period of the Keck observations are available but previous observations suggest the lightcurve amplitude is small and therefore not a significant source of error. In those cases in which no lightcurve data are available the uncertainties in the results are inevitably larger but the fact that the thermal continuum is measured over a period of typically 1 hour or more, at various wavelengths, results in a smoothing effect in the thermal-model fitting that tends to reduce the errors resulting from neglecting the rotational variability (for example, see the results for (5587) 1990 SB).

Uncertainties in thermal modeling usually exceed the formal errors resulting from the scatter of the flux measurements. In the case of NEATM, comparison with results from other sources, such as radar, indicate that overall errors are normally less than 15% in diameter and 30% in albedo. In those cases in which a default value of η was used, or the scatter of the flux values is large, the STM and FRM results can be taken as representing the limits of the uncertainty ranges for albedo and diameter.

The accuracy of albedo values derived via thermal models depends strongly on the accuracy of the adopted absolute magnitude, *H*. In those cases in which reliable *H* values are not available from other sources, we have resorted to estimates based on the values given by the JPL Horizons (ssd.jpl.nasa.gov/horizons.html), MPC (cfa-www.harvard.edu/iau/MPEph/MPEph.html), and NeoDys (newton.dm.unipi.it/neodys) web services. It should be noted that the uncertainty in these estimates is often large, e.g. ≥ 0.5 mag. In the event that more reliable *H* values become available in the future, the derived albedo and diameter values given in Table III can be updated using the convenient expressions given by Harris and Harris (1997).

The error bars in the plots of Fig. 1 reflect only the statistical uncertainties in the flux derivation from the synthetic aperture procedure. Lightcurve uncertainties, absolute calibration uncertainties, and differences in atmospheric transmission between measurements of the target and calibration star also contribute to the error budget.

5. COMMENTS ON INDIVIDUAL ASTEROIDS

The results in Table III should be viewed in conjunction with the following notes on individual objects. We note that for several objects, the measured albedo is a decisive parameter for determining a unique taxonomic class. In the taxonomic system of Tholen (1984) and Bus (1999), objects having neutral spectra within the X-complex typically display three categories of albedos. The "X" designation for an object is resolved into the classes E, M, or P based on its having a high, moderate, or low albedo, respectively. For the objects originally tabulated by Bus and Binzel (2002) or Binzel *et al*. (in preparation) as belonging to the X-complex, we indicate in Table III our resolution of the spectral degeneracy from X to (→) E, M, or P.

(1627) Ivar: The *H* value of 12.87 ± 0.1 is a new value from optical photometry by Pravec *et al*. (in preparation) made in the Spring of 2000, i.e. around the time of the Keck thermal-IR observations. The fluxes are lightcurve corrected (peak-to-peak amplitude = 0.35 mag). In the case of Ivar the lightcurve correction does not significantly improve the scatter of the flux values around the NEATM model thermal continuum; it does, however, significantly influence the resulting values of η, diameter and albedo. The NEATM fit can be improved somewhat by introducing a small phase shift in the lightcurve correction but the resulting value of η is heavily dependent on the magnitude of the shift. We note that the observations of this object were the first in our Keck program and the quality of the data may have been compromised by guiding problems. Since η is not well constrained by the measured flux values, the results given in Table III and plotted in Fig. 1 were obtained on the basis of the lightcurve-corrected fluxes, with no phase shift, and the default value of η of 1.0 for the NEATM fit. The present results for Ivar differ somewhat from those given in Table 2 of Harris and Lagerros (2002) due to the latter being based on a provisional analysis of the same data, which gave a lower value of η and a higher value of p_v. Ostro *et al*. (1990) conclude from their radar observations that Ivar has "a maximum dimension no less than 7 km and probably within 20% of 12 km", which is in good agreement with our results (D_{eff} = 9.1 km). The value of p_v from the present work (0.15) is consistent with Ivar's S classification and is in excellent agreement with that derived for Ivar by Kiselev *et al*. (1994) from polarimetry (0.14).

(1866) Sisyphus: The data are inadequate for spectral fitting. Only three reliable measurements were obtained, two at 11.7 μm and one at 12.5 μm. We have taken the weighted mean of these three flux values as a single point measurement corresponding to 12.0 μm. The NEATM results in Table III were obtained assuming a default value of η of 1.0. The albedo value of 0.15 is consistent with Sisyphus' S classification.

(2100) Ra-Shalom: A lightcurve correction has been applied to the fluxes plotted in Fig. 1. It is interesting to note that the effective diameter of 2.8 km is slightly larger, and the albedo of 0.082 somewhat lower, than the values obtained by Harris *et al*. (1998) from observations with the UK Infrared Telescope (see Table IV). However, the scatter of the Keck data is larger than that of the UKIRT data. In particular, the 4.8 μm point appears to be anomalously high (the presence of cirrus was noted on 2000 Aug. 21 UT, the night of the Keck observations of Ra-Shalom). Given the uncertainties, we consider the Keck and UKIRT results to be in reasonable agreement. Ra-Shalom has a C-type classification according to Tholen (1989) and an Xc classification according to Bus and Binzel (2002). We feel the available data for Ra-Shalom are not sufficiently unambiguous to allow further clarification of its taxonomic type at this stage.

(4034) 1986 PA: No lightcurve data are available for the time of the Keck observations. The source was weak in the thermal infrared and flux measurements in three filters only were made, which are inadequate for accurate determination of η. The results given in Table III for NEATM were obtained assuming a default value of η of 1.0. The results indicate a very high albedo. The taxonomic classification is O type (Binzel *et al*., in preparation).

(4055) Magellan: Reliable data were obtained in two filters only, due to the weakness of the fluxes. No lightcurve correction could be applied. The NEATM results in Table III were obtained assuming a default value of η of 1.0. The resulting albedo (0.31) is slightly higher than that (0.24) obtained by Harris (1998) using the NEATM on the 10 μm and 20 μm measurements of Cruikshank *et al*. (1991) but it is consistent with the V classification. (Harris, 1998, used a default η-value of 1.2; using this value with the Keck data results in an albedo of 0.26).

(4660) Nereus: No lightcurve data are available for the time of the Keck observations. The scatter of the flux values does not allow η to be adequately constrained, therefore the results given in Table III for NEATM were obtained assuming a default value for η of 1.5. The results indicate a very high albedo, which is consistent with refining the taxonomic type from Xe- to E-type.

(5587) 1990 SB: This case provides a good example of the effect of lightcurve correction of the thermal infrared fluxes. In Fig. 1b fluxes and model fits for (5587) are shown before and after lightcurve correction. The peak-to-peak amplitude of the lightcurve was 1.1 mag. Despite its dramatic effect in reducing the scatter of the flux values, the lightcurve correction in the case of (5587) does not greatly alter the derived value of diameter (the diameter derived from the NEATM fit to the uncorrected flux values is 3.08 km, cf. 3.57 km after correction). It was found that the scatter of the points about the NEATM model curve could be reduced to a minimum by introducing a small phase delay of 15 min. (18°) in the lightcurve correction. A delay between the optical and thermal-infrared lightcurves could be the result of thermal inertia and/or shape effects (cf. the optical and thermal-infrared lightcurves of (433) Eros obtained by Lebofsky and Rieke 1979). The phase shift had negligible effect on the results obtained from the model fits.

(5604) 1992 FE: This was one of the weakest sources observed. The three data points at 10.7 μm, 11.7 μm and 12.5 μm are inadequate for accurate determination of η, therefore the results given in Table III for NEATM were obtained assuming a default value of η of 1.0. Furthermore, no lightcurve information for the time of the Keck observations is available in this case. The value of *H* used, 17.72, is a new value derived from optical photometry obtained with the ESO 1.5-m Danish telescope (Delbó *et al.*, in preparation). Note that this value is about 1.3 mag fainter than that currently given by the JPL Horizons and MPC web sites. The high albedo value is consistent with the taxonomic classification as a V-type.

(5751) Zao: The results in Table III are based on three weak flux values. The default η-value of 1.5 was used for the NEATM. No lightcurve information is available for the time of our observations but the lightcurve amplitude is probably less than 0.15 mag (Pravec *et al*. 1997). The high albedo value allows us to refine the taxonomic type from X- to E-type.

(14402) 1991 DB: The value of *H* of 18.85 derives from the optical photometry of Pravec *et al*. (in preparation) made in the Spring of 2000, i.e. around the time of the Keck thermal-IR observations. The data quality is good with relatively little scatter about the NEATM model thermal continuum and the lightcurve has a low amplitude that can be neglected for the purposes of thermal-model fitting. Nevertheless, the NEATM albedo for this object (0.14) is higher than expected for a C spectral type. Only the FRM result would be compatible with the spectral type but as the plot in Fig. 1 shows, the FRM provides a very poor fit to the thermal fluxes: the observed disk-averaged surface color temperature is significantly higher than that of the FRM fit.

(16834) 1997 WU_{22}: A lightcurve correction has been applied to the fluxes plotted in Fig. 1 derived from the optical photometry of Pravec *et al*. (in preparation) made around the time of the Keck thermal-IR observations. The poor observing conditions on 2000 Aug. 21 UT are reflected in the large degree of scatter of the data points. The default η-value of 1.5 was used for the NEATM.

(19356) 1997 GH_3: No optical data are available for lightcurve correction, which increases the uncertainty associated with the results in Table III in this case. Nevertheless, the flux points show little scatter about the NEATM and STM continuum best fits and strongly exclude the FRM solution.

(25330) 1999 KV_4: No lightcurve correction is required due to the low amplitude of the lightcurve (~ 0.1 mag). The thermal model fits require a low albedo consistent with a B-type classification.

1999 FK_{21}: No lightcurve information is available for this object, which increases the uncertainty associated with the results in Table III in this case.

1999 NC_{43}: The solar phase angle and the value of η are both high in this case (59° and 2.86, respectively) and the disk-averaged color temperature appears to be as low as that of the FRM fit. Moreover, the lightcurve amplitude is very large (1.1 mag) indicating that the object has a very irregular form. It is possible that shadowing or shape effects may invalidate the application of simple thermal models in such cases (see Delbó and Harris 2002). Furthermore, the *H* value of this object is uncertain by about ± 0.5 mag due to the high phase angle at which the optical observations were made. While the

period of the lightcurve is not known (two solutions are possible on the basis of the observational data available), it is at least 34 h, which is much longer than the duration of our infrared observations. Therefore, for the purposes of calculating the diameter and albedo, we considered the infrared fluxes as having all been obtained at a single point in the rotation period and simply phase-corrected the *H* value accordingly. Unfortunately, due to there being two possible solutions for the period, two values of the phase-corrected *H* value are possible: 16.0 and 16.4, both with an uncertainty of ± 0.5 mag. For the entries in Table III we adopted $H = 16$, which leads to an albedo of 0.14 on the basis of the NEATM. This appears to be on the low side for a Q classification. However, the uncertainties in *H* would allow a value as bright as 15.5, which would give $p_v = 0.39$ on the basis of the FRM or $p_v = 0.23$ on the basis of the NEATM.

2000 BG_{19}: No lightcurve information is available for this object. Nevertheless, the data quality is good and the flux points show little scatter about the NEATM and STM continua best fits. Given the good quality of the NEATM and STM model fits it seems unlikely that the corresponding albedo values are grossly in error, implying that 2000 BG_{19} is a very dark asteroid. This low albedo allows the X taxonomic designation to be resolved, placing 2000 BG_{19} into the P-class.

2000 PG_3: This object was observed in poor conditions on 2000 Aug. 21 UT. The quality of the data does not allow η to be adequately constrained. Our optical photometry indicates that the lightcurve amplitude was negligible. The results given in Table III for NEATM were obtained assuming a default value for η of 1.0. The results from all three model fits indicate a very low albedo for this relatively large (~ 5 km) object that has a comet-like orbit. Our NEATM-derived albedo ($p_v = 0.042$) is typical for objects within the D-class but a factor of 2 higher than that obtained by Fernandez *et al*. (2001).

2001 FY: No lightcurve information is available for this object and the analysis is based on three very weak flux values only. The results given in Table III for NEATM were obtained assuming a default value for η of 1.0. The absence of lightcurve information increases the uncertainty associated with the results in this case.

2002 BM_{26}: Only incomplete lightcurve information is available for this object. Similar notes as for 2000 BG_{19} apply, except in this case the STM fit is very poor and the NEATM fit is much closer to that of the FRM. Indeed, given the large phase angle and unusually large value of η, there seems little reason to favor the NEATM solution over that of the FRM in this case (see Section 3). 2002 BM_{26} is reported to be a binary system on the basis of the radar observations of Nolan *et al.* (2002). The low albedo allows the X taxonomic designation to be resolved, placing 2002 BM_{26} into the P-class.

2002 CT_{46}: No lightcurve information is available for this object and the analysis is based on flux measurements made at two wavelengths only. The results given in Table III for NEATM were obtained assuming a default value of η of 1.0. The absence of lightcurve information increases the uncertainty associated with the results in this case.

6. DISCUSSION

Figure 2 shows a plot of η-value versus solar phase angle, based on the results of this study given in Table III and previously published results listed in Table IV. It is clear from Fig. 2 that in the case of NEAs the best-fit beaming parameter is normally significantly larger than the value η = 0.756 adopted by Lebofsky *et al*. (1986) for use in the STM. In our analysis of the distribution of the data plotted in Fig. 2 we have separated out the four points with $\eta > 2.0$, since the plot suggests these are in some way anomalous. The remaining points are scattered around the value $\eta = 1.25$, and suggest a trend of η increasing with increasing phase angle. We have used the distribution of the points with $\eta < 2.0$ to provide default best-guess values of η for those asteroids for which the data quality or quantity is inadequate to provide a reliable solution for η. The default values used are $\eta = 1.0$ for $\alpha < 45°$ and $\eta = 1.5$ for $\alpha > 45°$. If future observations confirm a trend of η increasing with phase angle, the relation could be used to provide more reliable estimates of η. It is instructive that the linear fit shown in Fig. 2 intersects the η axis at a value close to that adopted by Lebofsky *et al*. (1986) for use in the STM, implying that the STM may give reasonable results with NEAs *observed at small phase angles* in most cases.

[FIGURE 2]

Four data points in Fig. 2 (those labeled) are clearly significantly higher than the majority, indicating that the objects presented unusually low color temperatures to the observer. In these cases the FRM best fits to the observed thermal continua are reasonably good, suggesting the temperature distributions around the surfaces of the objects may be relatively smooth, with significant emission arising on the night side, due to high thermal inertia and/or high rotation rates. In this context we note that two of the three objects with the highest η-values, namely (3671) Dionysus and 2002 BM_{26}, are fast rotators with periods of around 2.7 h (however, the FRM solution for (3671) from Harris and Davies, 1999, requires $p_v > 0.3$, which is inconsistent with the taxonomic class Cb from Bus and Binzel 2002). On the other hand, the other two high-η objects, namely (2100) Ra-Shalom and 1999 NC_{43}, are *slow* rotators (with periods of 19.8 h and at least 34 h, respectively). Following Lebofsky and Spencer (1989), *if* their temperature distributions are well described by the FRM, Ra-Shalom and 1999 NC_{43} must have exceptionally high surface thermal inertias comparable to, or exceeding, that of solid rock (2500 J m^{-2} $s^{-0.5}$ K^{-1}, Jakosky 1986), respectively.

These latter results, and consideration of our dataset as a whole, suggest the above interpretation of the large η-values in terms of rotation rate and thermal inertia is an oversimplification. While the dataset is small, the plot of η versus phase angle in Fig. 2 raises the question of why no high-η objects (with the possible exception of (2100) Ra-Shalom) are observed at low or moderate phase angles. Our results suggest there may be another explanation for the high η values observed at large phase angles, other than fast rotation and/or high thermal inertia regolith-free surfaces. It may be relevant that two of the objects with the highest η-values, (3671) Dionysus and 2002 BM_{26}, are binary system candidates. Do binary NEAs have certain physical properties that lead to much lower than expected color temperatures being observed at high phase angles? Binary NEAs are thought to arise from the partial disruption of rubble piles passing close to a planet. Perhaps unusually rough or irregular surfaces, which could lead to a high degree of “beaming” of thermal radiation in the sunward direction and correspondingly less radiation being observed at high phase angles, are a characteristic of small rubble piles. If this were the case, we would expect such an object observed at a small phase angle to give rise to a correspondingly small value of η (high color temperature). Unfortunately, at the time of writing, no thermal-IR observations of a binary NEA at small phase angles are available to enable this hypothesis to be tested.

As noted in Section 5, in the case of 1999 NC_{43}, which has a high amplitude lightcurve indicative of a very irregular shape, the explanation for the high η value may lie in shape or shadowing effects that lead to less thermal emission being received from the observed parts of the surface than predicted by the spherical geometry on which the simple thermal models are based (see Delbó and Harris 2002). The importance of such effects increases with phase angle.

Another effect that probably contributes to the overall scatter of the points in Fig. 2 is the so-called "evening/morning" effect, in which the observed thermal emission of asteroids depends on which side of opposition they are observed on. An object viewed perpendicular to its rotation axis will present a lower color temperature to the observer if the rotation vector is such that the "morning" side, rather than the "evening" side, is observed. The magnitude of the effect depends on the thermal inertia and rate of rotation of an object, parameters that are normally unknown in the case of near-Earth asteroids.

Surface roughness, thermal inertia, shape, and rotation vector all contribute to the phase-angle dependence of the model parameter η, so modeling the effect of these phenomena on the observed thermal continua of NEAs without some prior knowledge of the surface structure and physical properties is very difficult with the current small database. However, further thermal-infrared observations will lead to clarification of this question and pave the way for quantitative modeling of the surface properties of NEAs.

The mean albedo of the 20 objects listed in Table III is 0.25. This is much higher than the mean albedo of main-belt asteroids listed in the IRAS Minor Planet Survey (Tedesco *et al*. 1992), which is around 0.1, although the significance of this comparison with the present small database for NEAs and possible observational bias is not clear. The albedos derived for the NEAs observed in the current study have a very broad range (0.02 – 0.55), which is entirely consistent with the spread of albedos for objects with diameters less than 30 km in the IRAS Minor Planet Survey. The objects observed in our study are much smaller than the asteroids in the population surveyed by IRAS. The apparent size dependence of asteroid albedos in the IRAS data has been discussed by a number of workers and attributed to the lack of a dusty regolith on small asteroids (see Tedesco 1993, and references therein). A rocky surface

should have a larger thermal inertia than that of a surface with a dusty regolith, thus causing the STM with its fixed value of 0.756 for the model parameter η to give erroneously high albedos. In Fig. 3 the albedos of 11 S-type asteroids from Tables III and IV are plotted against effective diameter. The albedos plotted in Fig. 3 are from the NEATM, which uses a variable η to take account of effects that may influence the observed color temperature, such as thermal inertia. Nevertheless, our data also suggest a trend of increasing albedo with decreasing size. While an observational bias against small dark objects in the NEA discovery surveys could also give rise to such a trend, we have minimized this effect by plotting the albedos of S-type asteroids only. Note also that our database contains several asteroids of other taxonomic classes in the size range 0.8 – 5 km with albedos below 0.1. We believe that the trend of increasing albedo with decreasing size is real and may be indicative, for example, of recently exposed, relatively unweathered surfaces. Note that these results are also consistent with the trend to ordinary-chondrite-type reflection spectra with decreasing size observed in the NEA population, which is also attributed to a lack of space weathering of relatively young surfaces (Binzel *et al*. 2002). For a detailed discussion of space weathering on asteroid surfaces see Clark *et al*. (2002).

[FIGURE 3]

Confirmation of the size dependence of albedos in the NEA population and its physical significance must await the results of further observations. However, we note here the importance of this issue for estimates of the size distribution of the NEA population, for which average albedos of 0.1 – 0.15 are normally assumed for the conversion of *H*-values to diameters. If actual albedos are higher than the assumed values, diameters corresponding to a given *H* distribution will be smaller.

7. CONCLUSIONS

We have derived the albedos and sizes of 20 near-Earth asteroids by fitting thermal-model continua to observed fluxes in the range 4.8 μm – 20 μm, thereby increasing the number of NEAs with measured albedos by 35%. The ambiguous taxonomic classifications of four asteroids have been clarified in the light of the new albedo values.

The mean albedo of the 20 objects observed is 0.25, which is much higher than the mean albedo of observed main-belt asteroids (~ 0.11). Our results are consistent with a trend of increasing albedo with decreasing size for S-type asteroids in the size range covered by our study (0.1 – 25 km). This could be at least partially due to an observational bias against small, dark objects, although we believe this is unlikely. Alternatively it may reflect the lack of space weathering of small, young collision fragments. Further data are required to confirm this.

2000 PG_3 is confirmed as a possible inactive cometary nucleus by virtue of its very low albedo. Agreement with the albedos expected from the taxonomic classifications is very good, with a few exceptions. (14402) 1991 DB has an albedo higher than that typical of a C-type asteroid, but it is not completely out of range for this category.

The model parameter, η, the so-called "beaming" parameter, is phase-angle dependent and significantly higher in general than the value 0.756 adopted by Lebofsky *et al.* (1986) in their version of the STM. However, we find that $\eta \sim 0.8$ appears to be valid at phase angles approaching zero, where the uncertainties associated with use of the STM are at a minimum, suggesting that the assumption of the STM of low thermal inertia (expected for an asteroid covered in dusty collisional debris) may be valid in most cases. The fact that our sample contains no object observed at a low phase angle for which η is large (> 1.2) suggests that NEAs with high thermal inertia (indicative of a rocky surface or course regolith) are relatively uncommon, although one of the objects among the NEAs observed to date that may have a high thermal inertia is (2100) Ra-Shalom (η = 2.3, α = 39°). On the other hand, the very large values of η obtained for three objects observed at high phase angles (~ 60°) may be due to unusual surface structure giving rise to a strong sunward beaming effect and/or shape effects causing shadowing, rather than high thermal inertia. However, further work is required to enable observed values of the beaming parameter to be reliably interpreted in terms of the physical properties of NEAs.

ACKNOWLEDGMENTS

The data presented herein were obtained at the W.M. Keck Observatory, which is operated as a scientific partnership among the California Institute of Technology, the University of California and the National Aeronautics and Space Administration. The Observatory was made possible by the generous financial support of the W.M. Keck Foundation. We would like to thank the staff of the Keck Observatory, in particular Greg Wirth and Randy Campbell, for their hospitality and support during our observing runs. The comments and suggestions of Mark Sykes and an anonymous referee are gratefully acknowledged. The work of M. Delbó was supported by the Deutsche Forschungsgemeinschaft (DFG). The work of P. Pravec was supported by the Grant Agency of the Czech Republic, Grant 205-99-0255, and by the Grant Agency of the Academy of Sciences of the Czech Republic, Grant A3003204.

REFERENCES

Binzel, R. P., D. F. Lupishko, M. Di Martino, R. J. Whiteley, and G. Hahn 2002. Physical properties of near-Earth objects. In *Asteroids III* (W. Bottke, A. Cellino, P. Paolicchi, and R. P. Binzel, Eds.), pp. 255–271. Univ. of Arizona Press, Tucson.

Binzel, R. P., M. Birlan, S. J. Bus, A. W. Harris, A. S. Rivkin, and S. Fornasier 2003. Spectral observations for near-Earth objects including potential target 4660 Nereus: Results from Meudon remote observations at the NASA Infrared Telescope Facility (IRTF). Submitted to *Planetary and Space Science*.

Bottke, W. F., R. Jedicke, A. Morbidelli, J.-M. Petit, B. Gladman 2000. Understanding the distribution of near-Earth asteroids. *Science* **288**, 2190–2194.

Bus, S. J. 1999. *Compositional structure in the asteroid belt: Results of a spectroscopic survey.* Doctoral thesis, Massachusetts Institute of Technology.

Bus, S. J., and R. P. Binzel 2002. Phase II of the Small Main-Belt Asteroid Spectroscopic Survey: A feature-based taxonomy. *Icarus* **158**, 146–177.

Clark, B. E., B. Hapke, C. Pieters, and D. Britt 2002. Asteroid space weathering and regolith evolution. In *Asteroids III* (W. Bottke, A. Cellino, P. Paolicchi, and R. P. Binzel, Eds.), pp. 585–599. Univ. of Arizona Press, Tucson.

Cohen, M., R. G. Walker, B. Carter, P. Hammersley, M. Kidger, and K. Noguchi 1999. Spectral irradiance calibration in the infrared. X. A self-consistent radiometric all-sky network of absolutely calibrated stellar spectra. *Astron. J.* **117**, 1864 – 1889.

Cruikshank, D. P., D. J. Tholen, W. K. Hartmann, J. F. Bell, and R. H. Brown 1991. Three basaltic Earth-approaching asteroids and the source of the basaltic meteorites. *Icarus* **89**, 1–13.

Delbó, M., and A. W. Harris 2002. Physical properties of near-Earth asteroids from thermal infrared observations and thermal modeling. *Meteoritics and Plan. Sci.* **37**, 1929–1936.

Fernandez, Y. R., D. C. Jewitt, and S. S. Sheppard 2001. Low albedos among extinct comet candidates. *Ap. J. Lett.* **553**, L197–L200.

Harris, A. W. 1998. A thermal model for near-Earth asteroids. *Icarus* **131**, 291–301.

Harris, A. W., and J. K. Davies 1999. Physical characteristics of near-Earth asteroids from thermal infrared spectrophotometry. *Icarus* **142**, 464–475.

Harris, A. W., and A. W. Harris 1997. On the revision of radiometric albedos and diameters of asteroids. *Icarus* **126**, 450–454.

Harris, A. W., and J. S. V. Lagerros 2002. Asteroids in the thermal infrared. In *Asteroids III* (W. Bottke, A. Cellino, P. Paolicchi, and R. P. Binzel, Eds.), pp. 205–218. Univ. of Arizona Press, Tucson.

Harris, A. W., J. K. Davies, and S. F. Green 1998. Thermal infrared spectrophotometry of the near-Earth asteroids 2100 Ra-Shalom and 1991 EE. *Icarus* **135**, 441–450.

Jakosky, B. M. 1986. On the thermal properties of Martian fines. *Icarus* **66**, 117–124.

Jones, B., and R. C. Puetter 1993. In *Infrared Detectors and Instrumentation* (A. M. Fowler, Ed.), Proc. SPIE, **1946**, pp. 610 - 621.

Kiselev, N.N., G. P. Chernova, and D. F. Lupishko 1994. Polarimetry of asteroids 1036 Ganymed and 1627 Ivar. *Kinematika. Fiz. Nebesnyka Tel* **10**(2), 35 – 39.

Lebofsky, L. A., and G. H. Rieke 1979. Thermal properties of 433 Eros. *Icarus* **40**, 297–308.

Lebofsky, L. A., and J. R. Spencer 1989. Radiometry and thermal modeling of asteroids. In *Asteroids II* (R. P. Binzel, T. Gehrels, and M. S. Matthews, Eds.), pp. 128 - 147. Univ. of Arizona Press, Tucson.

Lebofsky, L. A., M. V. Sykes, E. F. Tedesco, G. J. Veeder, D. L. Matson, R. H. Brown, J. C. Gradie, M. A. Feierberg, and R. J. Rudy 1986. A refined "standard" thermal model for asteroids based on observations of 1 Ceres and 2 Pallas. *Icarus* **68**, 239–251.

Nolan, M. C., E. S. Howell, C. Magri, B. Beeney, D. B. Campbell, L. A. M. Benner, S. J. Ostro, J. D. Giorgini, and J.-L. Margot 2002. *2002 BM_{26}.* IAU Circ. 7824.

Ostro, S. J., D. B. Campbell, A. A. Hine, I. I. Shapiro, J. F. Chandler, C. L. Werner, and K. D. Rosema 1990. Radar images of asteroid 1627 Ivar. *Astron. J.* **99**, 2012–2018.

Pravec, P., M. Wolf, L. Sarounova, S. Mottola, A. Erikson, G. Hahn, A. W. Harris, A. W. Harris, and J. W. Young 1997. The near-Earth objects follow-up program II. Results for 8 asteroids from 1982 to 1995. *Icarus* **130**, 275–286.

Stuart, J. S. 2001. A near-Earth asteroid population estimate from the LINEAR survey. *Science*, **294**, 1691–1693.

Tedesco, E. F. (ed.) (1992) *The IRAS Minor Planet Survey.* Tech. Rep. PL-TR-92-2049. Phillips Laboratory, Hanscom Air Force Base, MA.

Tedesco, E. F. 1993. Asteroid albedos and diameters. *Proc. IAU Symp. 160, Asteroids, Comets, Meteors* (A. Milani, M. Di Martino, and A. Cellino, Eds.), pp. 55 - 74. Kluwer, Dordrecht.

Tholen, D. J. 1984. *Asteroid taxonomy from cluster analysis of photometry*. Doctoral thesis, University of Arizona.

Tholen, D. J. 1989. Asteroid taxonomic classifications. In *Asteroids II* (R. P. Binzel, T. Gehrels, and M. S. Matthews, Eds.), pp. 1139 - 1150. Univ. of Arizona Press, Tucson.

Veeder, G. J., M. S. Hanner, D. L. Matson, E. F. Tedesco, L. A. Lebofsky, and A. T. Tokunaga 1989. Radiometry of near-Earth asteroids. *Astron. J*. **97**, 1211 - 1219.

Werner, S. C., A. W. Harris, G. Neukum, B. A. Ivanov 2002. NOTE: The near-Earth asteroid size-frequency distribution: A snapshot of the lunar impactor size-frequency distribution. *Icarus*, **156,** 287 - 290.

TABLE I

Observational Circumstances and Relevant Data

Object	*H* (mag)	Date	*α*°	*R* (AU)	*Δ* (AU)	Lightcurve Per. (h)	Lightcurve amp. (mag)	Notes
1627 Ivar	12.87±0.1	00-03-16	5	2.057	1.073	4.795	0.35	1
1866 Sisyphus	13.00	00-03-17	16	2.903	2.194	2.400	0.11	2
2100 Ra-Shalom	16.11±0.1	00-08-21	39	1.175	0.222	19.79	0.40	1
4034 1986 PA	18.2	01-05-11	40	1.219	0.299	-	-	
4055 Magellan	14.9±0.2	00-03-16	13	2.058	1.122	7.475	0.46	1
4660 Nereus	18.7	02-02-21	60	1.033	0.093	15.1	0.6	2
5587 1990 SB	14.1±0.5	01-05-10	42	1.213	0.301	5.052	1.1	1
5604 1992 FE	17.72	01-05-11	36	1.301	0.392	-	-	3
5751 Zao	14.93±0.07	01-05-12	49	1.250	1.180	≥ 21.7	0.12	4
14402 1991 DB	18.85±0.1	00-03-16	36	1.076	0.103	2.266	~0.1	1
16834 1997 WU_{22}	15.9±0.5	00-08-21	59	1.142	0.331	9.348	0.4	1
19356 1997 GH_3	17.0	01-05-11	5	1.421	0.413	6.714	0.74	2
25330 1999 KV_4	16.3	01-05-10	54	1.201	0.425	4.90	~0.1	
1999 FK_{21}	18.0	02-02-21	35	1.142	0.195	-	-	
1999 NC_{43}	16.1±0.5	00-03-17	59	1.130	0.366	34.5/122.3?	1.1	1
2000 BG_{19}	17.8	00-03-17	17	1.396	0.429	-	-	
2000 PG_3	15.74	00-08-21	2	2.118	1.108	-	≤ 0.2	
2001 FY	18.8	01-05-12	22	1.269	0.285	-	-	
2002 BM_{26}	20.1	02-02-21	60	1.024	0.074	~ 2.7	-	5
2002 CT_{46}	20.8	02-02-21	23	1.107	0.129	-	-	

Notes.

1. Lightcurve data and mean *H* derived from photometry made during the apparition of the Keck thermal observations by Pravec and colleagues. In the cases of (5587), (16834), and 1999 NC_{43} only rough *H*-values could be estimated due to the high phase angle of the observations.

2. Lightcurve data from the compilation of (the other) A. W. Harris, version 2001 March 1 (cfa-www.harvard.edu/iau/lists/LightcurveDat.html).

3. *H*-value from Delbó *et al*. (in preparation), from observations carried out at the European Southern Observatory, La Silla.

4. Lightcurve data and mean *H* taken from Pravec *et al*. (1997). The *H*-value should also be valid for the 2001 apparition to an accuracy of ~0.1 mag as the asteroid showed little aspect-related variation in earlier apparitions.

5. Rotational period of ~ 2.7 h from Nolan *et al*. (2002).

Remaining *H*-values are from the web services given in Section 4 or, in the cases of (1866) and (4660), A. W. Harris (priv. comm.).

TABLE II

Observed Fluxes

Object	Date	Time (UT)	Wave-Length (μm)	Flux (mJy)	Error (mJy)	Flux X 10^{-14} ($Wm^{-2}\mu m^{-1}$)	Flux Error X 10^{-14} ($Wm^{-2}\mu m^{-1}$)
1627 Ivar	00-03-16	10:39:38	8.0	150	8	0.7026	0.0375
		11:01:54	8.9	199	6	0.7532	0.0227
		09:39:49	10.7	294	10	0.7698	0.0262
		09:44:50	10.7	287	9	0.7515	0.0236
		09:54:08	11.7	421	7	0.9220	0.0153
		10:01:23	12.5	380	7	0.7291	0.0134
		10:25:03	20.0	705	22	0.5284	0.0165
1866 Sisyphus	00-03-17	16:12:39	11.7	36	4	0.0788	0.0088
		15:25:32	11.7	46	4	0.1007	0.0088
		15:33:30	12.5	26	4	0.0499	0.0077
2100 Ra-Shalom	00-08-21	10:27:44	4.8	66	6	0.8588	0.0781
		10:22:43	8.9	567	10	2.1459	0.0378
		10:17:05	11.7	1172	20	2.5667	0.0438
		10:36:13	20.0	1421	57	1.0650	0.0427
4034 1986 PA	01-05-11	08:13:15	10.7	23	3	0.0602	0.0079
		08:00:19	11.7	25	3	0.0547	0.0066
		08:25:42	12.5	22	3	0.0422	0.0058
4055 Magellan	00-03-16	14:50:21	10.7	15	4	0.0393	0.0105
		14:39:48	11.7	30	4	0.0657	0.0088
4660 Nereus	02-02-21	16:02:11	8.0	80	8	0.3747	0.0375
		15:27:49	8.9	65	4	0.2460	0.0151
		14:58:54	10.7	107	4	0.2802	0.0105
		14:25:52	11.7	80	4	0.1752	0.0088
		14:35:31	11.7	109	6	0.2387	0.0131
		15:11:20	11.7	98	5	0.2146	0.0109
		14:43:20	12.5	98	5	0.1880	0.0096
		15:45:10	17.65	104	16	0.1001	0.0154
5587 1990 SB	01-05-10	09:11:59	4.8	164	4	2.1339	0.0520
		09:48:49	4.8	175	5	2.2770	0.0651
		09:00:00	8.0	993	22	4.6514	0.1031
		08:53:40	8.9	1053	22	3.9853	0.0833
		08:48:54	10.7	1275	27	3.3385	0.0707
		09:43:01	11.7	2698	46	5.9086	0.1007
		08:41:32	11.7	1432	24	3.1361	0.0526
		09:05:50	12.5	2083	44	3.9965	0.0844
		10:02:17	17.9	2472	80	2.3129	0.0749

		09:28:38	17.9	2571	81	2.4055	0.0758
		09:35:53	20.0	2972	95	2.2274	0.0712
5604 1992 FE	01-05-11	06:49:49	10.7	14	2	0.0367	0.0052
		06:24:34	11.7	22	3	0.0482	0.0066
		06:36:50	12.5	27	3	0.0518	0.0058
5751 Zao	01-05-12	06:28:49	10.7	18	1	0.0471	0.0026
		06:04:22	11.7	34	1	0.0745	0.0022
		06:16:39	12.5	23	2	0.0441	0.0038
14402 1991 DB	00-03-16	13:26:01	4.8	46	3	0.5985	0.0390
		13:17:43	8.0	368	16	1.7238	0.0749
		13:13:03	8.9	445	14	1.6842	0.0530
		13:08:33	10.7	622	11	1.6287	0.0288
		13:03:30	11.7	682	12	1.4936	0.0263
		13:21:45	12.5	640	12	1.2279	0.0230
		13:58:10	20.0	513	21	0.3845	0.0157
		13:49:07	20.0	507	24	0.3800	0.0180
16834 1997 WU_{22}	00-08-21	07:12:10	8.0	133	11	0.6230	0.0515
		07:05:13	8.9	156	5	0.5904	0.0189
		07:58:41	10.7	252	9	0.6599	0.0236
		07:20:58	11.7	351	8	0.7687	0.0175
		06:42:47	11.7	264	8	0.5782	0.0175
		06:47:00	12.5	283	7	0.5430	0.0134
19356 1997 GH_3	01-05-11	09:05:36	8.9	41	4	0.1552	0.0076
		08:53:11	10.7	50	2	0.1309	0.0052
		09:57:02	11.7	59	2	0.1292	0.0044
		08:41:05	11.7	63	2	0.1380	0.0044
		09:30:59	12.5	63	2	0.1209	0.0038
		09:43:55	17.9	74	12	0.0692	0.0112
25330 1999 KV_4	01-05-10	07:11:05	4.8	35	5	0.4554	0.0651
		07:04:25	8.0	250	12	1.1710	0.0562
		06:55:43	8.9	292	9	1.1051	0.0341
		06:51:05	10.7	394	12	1.0317	0.0314
		06:19:41	11.7	520	16	1.1388	0.0350
		06:43:14	11.7	506	15	1.1081	0.0328
		07:21:34	17.9	629	35	0.5885	0.0327
		07:35:43	20.0	643	33	0.4819	0.0247
		07:28:11	20.0	563	32	0.4220	0.0240
1999 FK_{21}	02-02-21	11:14:08	8.9	115	5	0.4352	0.0189
		11:47:22	11.7	164	6	0.3592	0.0131
		10:50:23	11.7	167	7	0.3657	0.0153
		11:01:48	12.5	142	6	0.2724	0.0115

		11:26:59	17.65	198	13	0.1905	0.0125
1999 NC_{43}	00-03-17	07:18:18	8.9	93	5	0.3520	0.0189
		07:29:37	10.7	113	3	0.2959	0.0079
		06:35:46	11.7	173	4	0.3789	0.0088
		07:37:02	11.7	154	4	0.3373	0.0088
		07:57:03	11.7	151	3	0.3307	0.0066
		06:40:35	12.5	171	4	0.3281	0.0077
		06:58:08	20.0	207	16	0.1551	0.0120
		06:48:27	20.0	256	19	0.1919	0.0142
2000 BG_{19}	00-03-17	10:54:00	4.8	29	4	0.3773	0.0520
		11:07:05	8.9	214	7	0.8099	0.0265
		11:18:41	10.7	279	8	0.7305	0.0209
		11:26:22	11.7	340	10	0.7446	0.0219
		10:18:15	11.7	344	10	0.7534	0.0219
		10:26:34	12.5	303	9	0.5813	0.0173
		10:46:50	20.0	321	25	0.2406	0.0187
		10:35:13	20.0	304	28	0.2278	0.0210
2000 PG_3	00-08-21	09:55:45	8.0	47	6	0.2202	0.0281
		09:41:40	8.9	55	2	0.2082	0.0076
		09:13:28	10.7	69	2	0.1807	0.0052
		09:04:42	11.7	120	3	0.2628	0.0066
		09:20:53	12.5	108	3	0.2072	0.0058
2001 FY	01-05-12	09:02:13	10.7	14	1	0.0367	0.0026
		08:34:36	11.7	21	2	0.0460	0.0044
		08:47:15	12.5	15	2	0.0288	0.0038
2002 BM_{26}	02-02-21	08:41:25	8.0	260	12	1.2179	0.0562
		08:36:45	8.9	335	8	1.2679	0.0303
		09:02:08	11.7	708	15	1.5505	0.0328
		08:27:36	11.7	710	15	1.5549	0.0328
		08:05:46	11.7	680	14	1.4892	0.0307
		08:31:58	12.5	687	14	1.3181	0.0269
		08:51:43	17.65	894	21	0.8603	0.0202
2002 CT_{46}	02-02-21	13:25:55	10.7	15	3	0.0393	0.0079
		14:12:53	11.7	43	3	0.0942	0.0066
		12:39:18	11.7	30	2	0.0657	0.0044
		13:13:17	11.7	27	2	0.0586	0.0043

TABLE III

Diameters and Albedos from Thermal-Model Fits

Object	D_{eff} (km)				p_v			Tax. Class	Notes
	STM	NEATM	η	FRM	STM	NEATM	FRM		
1627 Ivar	7.94	**9.12**	(1.0)	15.9	0.20	**0.15**	0.050	S	Lc corrected
1866 Sisyphus	7.47	**8.48**	(1.0)	16.3	0.20	**0.15**	0.042	S	Lc amp. small
2100 Ra-Shalom	1.59	**2.78**	2.32	2.59	0.25	**0.082**	0.095	Xc	Lc corrected
4034 1986 PA	0.40	**0.42**	(1.0)	0.57	0.58	**0.52**	0.29	O	
4055 Magellan	2.20	**2.49**	(1.0)	4.36	0.39	**0.31**	0.10	V	
4660 Nereus	0.26	**0.33**	(1.5)	0.33	0.86	**0.55**	0.54	Xe → E	
5587 1990 SB	3.38	**3.57**	0.93	5.03	0.35	**0.32**	0.16	Sq	Lc corrected
5604 1992 FE	0.52	**0.55**	(1.0)	0.77	0.53	**0.48**	0.25	V	
5751 Zao	1.80	**2.30**	(1.5)	2.53	0.58	**0.36**	0.29	X → E	Lc amp. small
14402 1991 DB	0.56	**0.60**	1.04	0.81	0.17	**0.14**	0.08	C	Lc amp. small
16834 1997 WU_{22}	1.39	**1.87**	(1.5)	1.92	0.40	**0.22**	0.21	S	Lc corrected
19356 1997 GH_3	0.83	**0.91**	0.98	1.45	0.41	**0.34**	0.13	S	
25330 1999 KV_4	2.34	**3.21**	1.50	3.41	0.098	**0.052**	0.046	B	Lc amp. small
1999 FK_{21}	0.58	**0.59**	0.91	0.85	0.33	**0.32**	0.15	S	
1999 NC_{43}	1.22	**2.22**	2.86	**1.62**	0.47	**0.14**	**0.27**	Q	Lc corrected
2000 BG_{19}	1.88	**1.77**	0.74	3.25	0.038	**0.043**	0.013	X → P	
2000 PG_3	3.90	**4.60**	(1.0)	8.59	0.059	**0.042**	0.012	D	Lc amp. small
2001 FY	0.30	**0.32**	(1.0)	0.48	0.59	**0.52**	0.23	S	
2002 BM_{26}	0.41	**0.84**	3.10	**0.57**	0.094	**0.023**	**0.050**	X → P	
2002 CT_{46}	0.15	**0.16**	(1.0)	0.24	0.36	**0.32**	0.15	Sr	

Notes. The diameter and albedo values printed in bold type are considered to be the most reliable in each case judging from the thermal-model fits, with the provisos given in Section 5. The estimated overall uncertainties in the NEATM values of diameter and albedo are 15% and 30%, respectively (see Section 4). Differences to the results tabulated by Harris and Lagerros (2002) are due to the use of updated parameters and a more detailed analysis in the present work. D_{eff} is the diameter of a sphere presenting the same projected area to the observer. Values of η in brackets are phase-angle dependent default values chosen on the basis of the results shown in Fig. 2. The results in this table should be viewed in conjunction with the notes on individual objects in Section 5. Taxonomic classes are from Bus and Binzel (2002) and the results of Binzel *et al*. (in preparation), with the exceptions of (4055) Magellan (Cruikshank *et al*. 1991) and (4660) Nereus (Binzel *et al*. 2003).

TABLE IV

Previously Published Results

Object	NEATM			*H* (mag)	α°	Tax. Class
	Diameter (km)	p_v	η			
433 Eros	23.6 (lc max.)	0.20	1.05	10.47 (lc max.)	10	S
	23.6 (lc max.)	0.21	1.07		31	
	14.3 (lc min.)	0.22	1.15	11.50 (lc min.)	10	
1862 Apollo	1.4	0.26	1.15	16.27	35	Q
1980 Tezcatlipoca	6.7 (lc max.)	0.14	1.54	13.60 (lc max.)	63	Sl
	6.6 (lc max.)	0.15	1.64		63	
2100 Ra-Shalom	2.5 (lc max.)	0.13	1.80	15.90 (lc max.)	41	Xc
3200 Phaethon	5.1	0.11	1.60	14.51	48	B
3554 Amun	2.1	0.17	1.20	15.94	16	M
3671 Dionysus	1.5	0.16	3.1	16.66	58	Cb
9856 1991 EE	1.0	0.30	1.15	16.90	36	S

Notes. Original data sources:

(433), (1980), (3671): see Harris and Davies (1999);

(1862), (3200), (3554): see Harris (1998);

(2100), (9856): Harris *et al*. (1998).

Taxonomic classes are from Bus and Binzel (2002) or Binzel *et al*. (2002). For (3671) we have taken the NEATM solution requiring η = 3.1 (see Harris and Davies 1999). The FRM also provides a reasonable fit to the data for (3671) but it gives a much higher albedo of 0.30 – 0.35, which is seriously inconsistent with the taxonomic type of Bus and Binzel (2002).

FIGURE CAPTIONS

1a (11 frames). Weighted thermal-model fits to the flux values listed in Table II. The curves represent the standard thermal model with parameters as given by Lebofsky *et al*. (1986) (STM - continuous), the near-Earth asteroid thermal model (NEATM - dotted), and the fast rotating model (FRM - dashed). The model curves are best fits generated by finding the values of diameter and albedo (and η in the case of NEATM) that minimize $\sum[(F_n(\text{obs}) - F_n(\text{model}))/\sigma_n]^2$, where σ_n are the statistical uncertainties in the photometry, $F_n(\text{obs})$. In those cases in which the data quality are inadequate for a reliable determination of η, default values of η = 1.0 (phase angle < 45°) and η = 1.5 (phase angle > 45°) were used, based on the results shown in Fig. 2. Note that the error bars reflect only the statistical uncertainties in the flux derivation from the synthetic aperture procedure. Lightcurve uncertainties, absolute calibration uncertainties, and varying atmospheric transmission contribute to the scatter of the data.

1b. Weighted thermal-model fits to the flux values of (5587) 1990 SB. The flux data are plotted before lightcurve correction (left-hand frame) and after normalizing to the mean lightcurve magnitude, to illustrate the resulting dramatic reduction in the scatter of the points. For other details refer to the caption to Fig. 1a.

2. Best-fit beaming parameter, η, from the NEATM fits plotted against solar phase angle, α. The error bars represent a conservative 20% uncertainty, which is based on the reproducibility of η for those objects for which more than one measurement from independent data sets is available (see Tables III and IV). The line represents a linear fit ($\eta = 0.81 + 0.01\alpha$) to those values below 2.0. The four values above 2.0 are considered to be anomalously high (see text) and were excluded from the fit. Significant deviations of η from the linear fit may be due to the effects of unusually high or low thermal inertia and/or surface roughness, and/or an irregular shape, influencing the surface temperature distribution presented to the observer. The “evening/morning” effect probably contributes to the scatter of the points (see text).

3. Plot of geometric albedo versus diameter for S-type asteroids in Tables III and IV. Conservative error bars are shown at the ±30% level in albedo and ±15% level in diameter, which are the estimated overall uncertainties associated with use of the NEATM. The plot suggests a significant trend of increasing albedo with decreasing size. The trend may be due to an observational bias against small, dark objects, or a lack of high albedo objects at larger sizes (see text).

Figure 1a (11 frames):

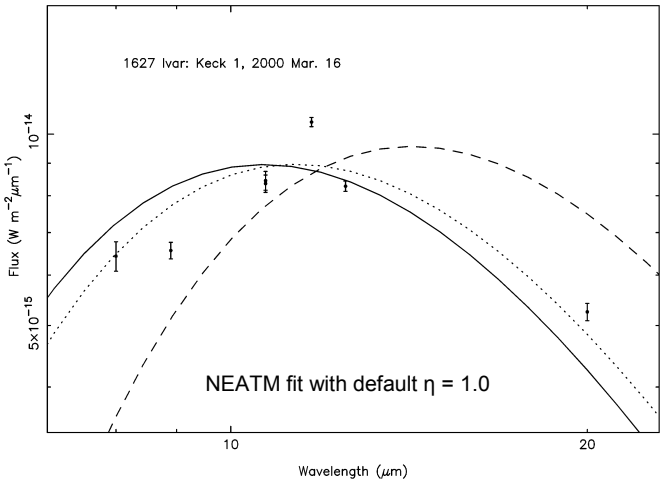

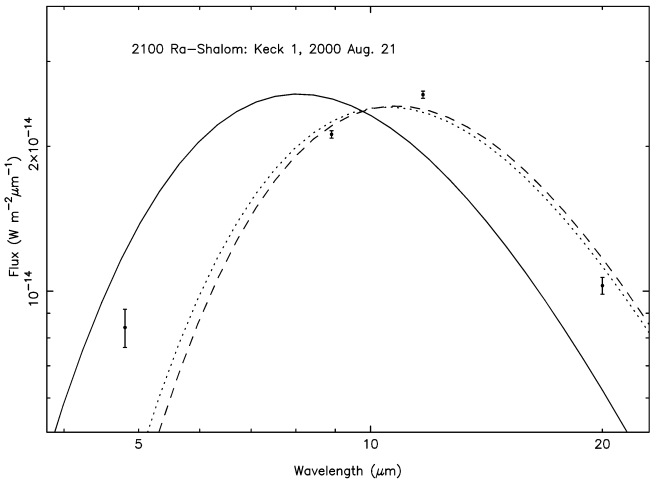

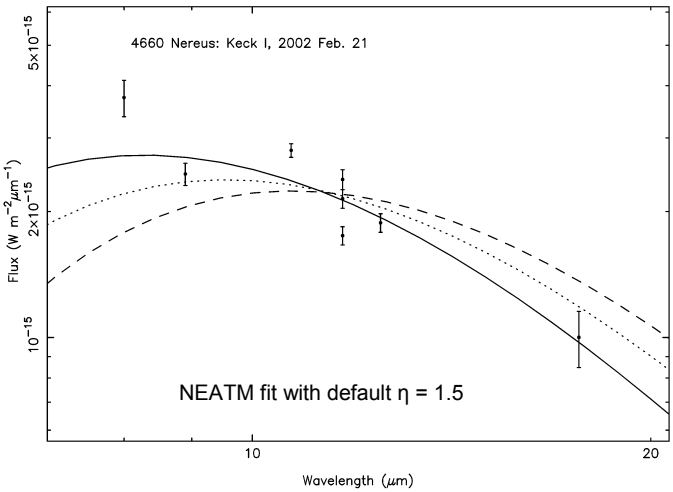

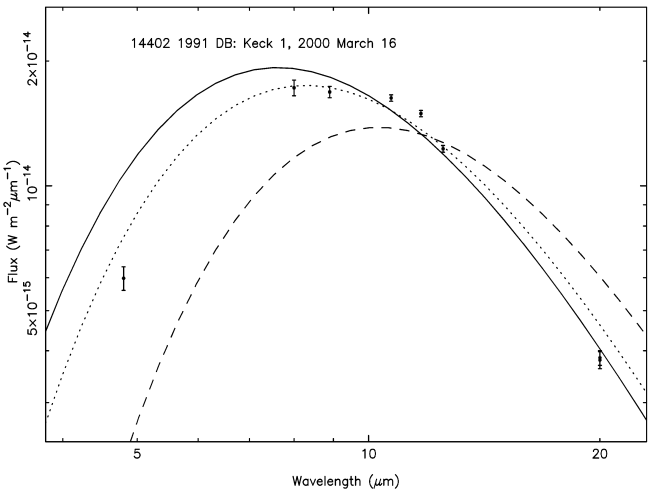

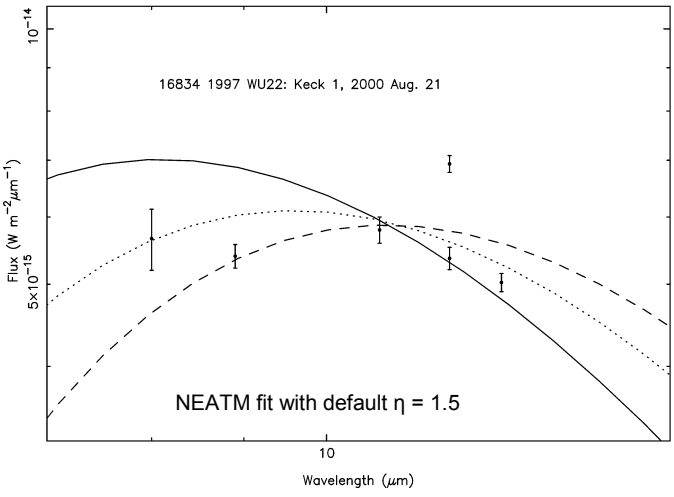

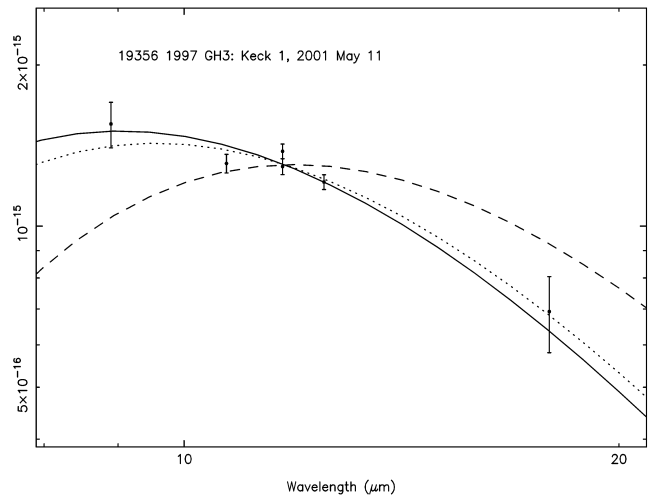

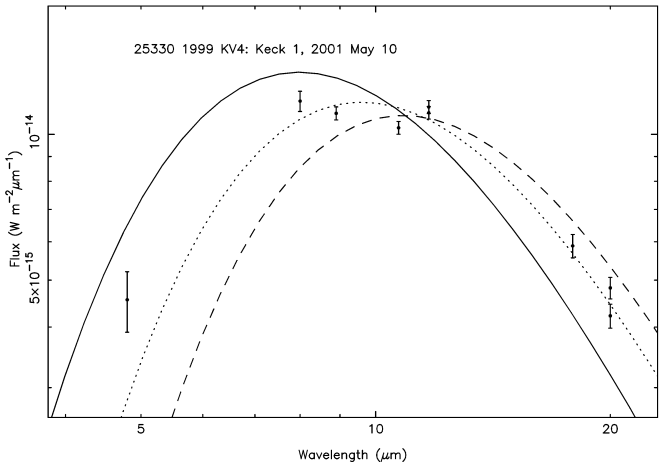
25330 1999 KV4: Keck 1, 2001 May 10
Flux (W m$^{-2}\mu$m^{-1})
10^{-14}
5×10^{-15}
5
10
20
Wavelength (μm)

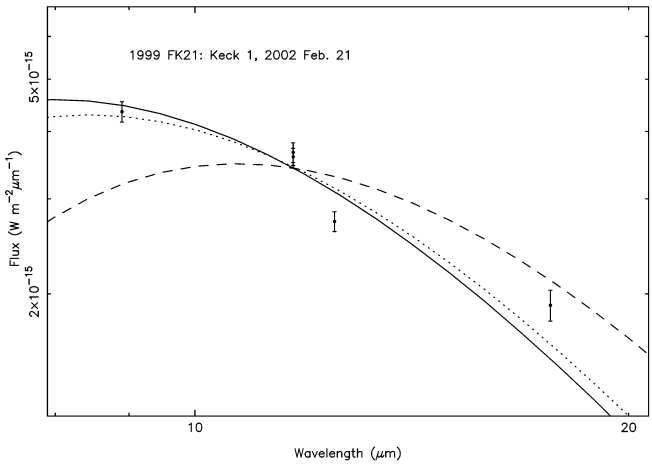
1999 FK21: Keck 1, 2002 Feb. 21
Flux (W m$^{-2}\mu$m^{-1})
5×10^{-15}
2×10^{-15}
10
20
Wavelength (μm)

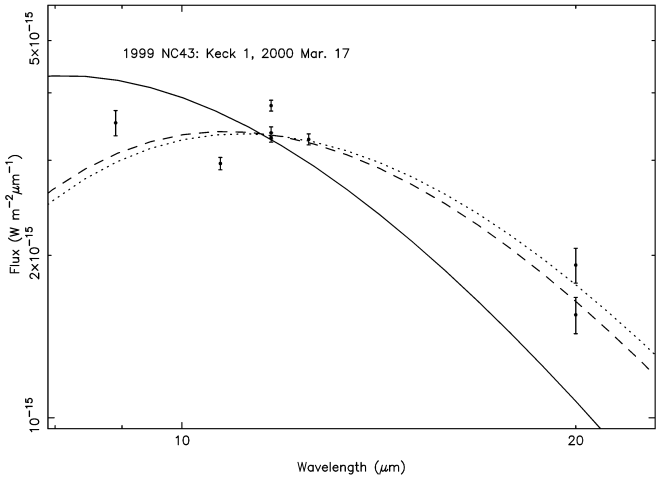
1999 NC43: Keck 1, 2000 Mar. 17
Flux (W m$^{-2}\mu$m^{-1})
5×10^{-15}
2×10^{-15}
10^{-15}
10
20
Wavelength (μm)

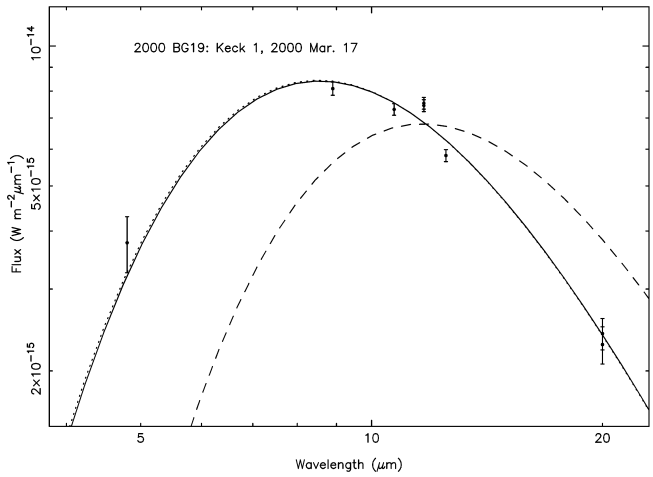
2000 BG19: Keck 1, 2000 Mar. 17
Flux (W m$^{-2}\mu$m^{-1})
10^{-14}
5×10^{-15}
2×10^{-15}
5
10
20
Wavelength (μm)

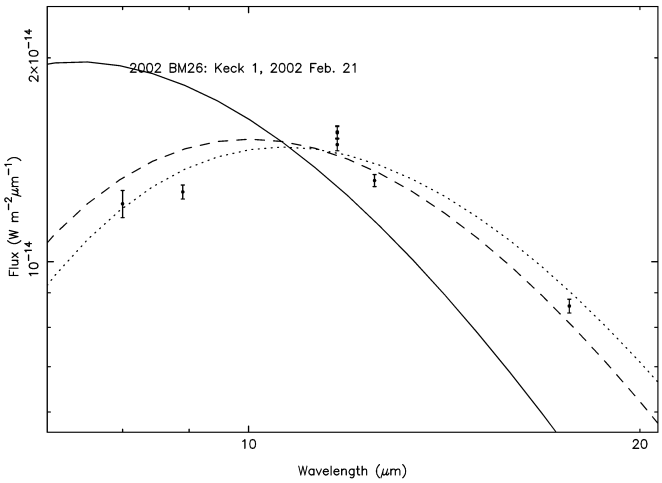
2002 BM26: Keck 1, 2002 Feb. 21
Flux (W m$^{-2}\mu$m^{-1})
2×10^{-14}
10^{-14}
10
20
Wavelength (μm)

Figure 1b:

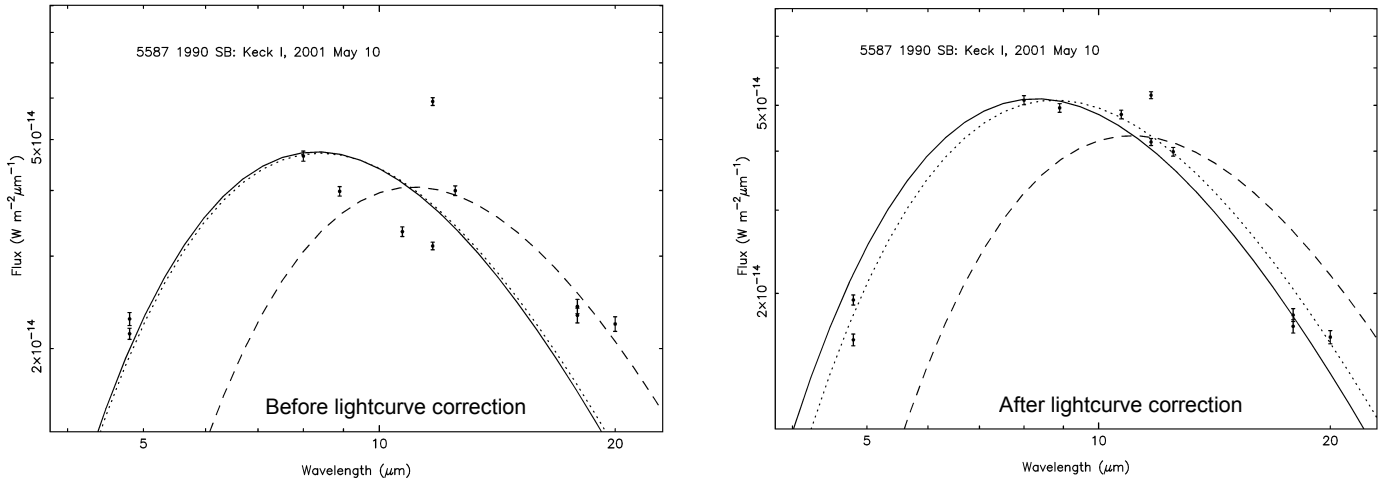
5587 1990 SB: Keck I, 2001 May 10
Flux (W m^{-2} μm^{-1})
5×10^{-14}
2×10^{-14}
Before lightcurve correction
5
10
20
Wavelength (μm)
5587 1990 SB: Keck I, 2001 May 10
Flux (W m^{-2} μm^{-1})
5×10^{-14}
2×10^{-14}
After lightcurve correction
5
10
20
Wavelength (μm)

Figure 2:

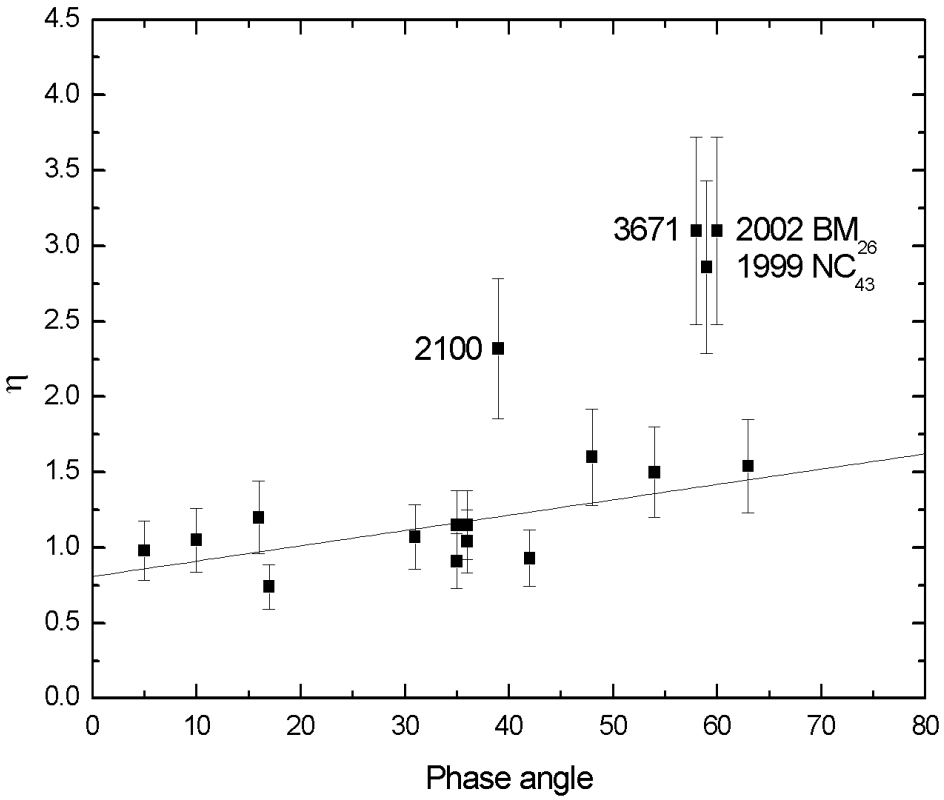
4.5
4.0
3.5
3.0
2.5
2.0
1.5
1.0
0.5
0.0
η
0
10
20
30
40
50
60
70
80
Phase angle
3671
2002 BM26
1999 NC43
2100

Figure 3: